

Programmable quantum simulations on a trapped-ions quantum computer with a global drive

Yotam Shapira^{1,*}, Jovan Markov^{1,*}, Nitzan Akerman¹, Ady Stern², and Roei Ozeri¹

¹Department of Physics of Complex Systems, Weizmann Institute of Science, Rehovot 7610001, Israel

² Department of Physics of Condensed Matter Systems,
Weizmann Institute of Science, Rehovot 7610001, Israel

* These authors contributed equally to this work

Simulation of quantum systems is notoriously challenging for classical computers, while quantum computers are naturally well-suited for this task. However, the imperfections of contemporary quantum computers pose a considerable challenge in carrying out accurate simulations over long evolution times. Here we experimentally demonstrate a method for quantum simulations on a small-scale trapped ions-based quantum computer. Our method enables quantum simulations of programmable spin-Hamiltonians, using only simple global fields, driving all qubits homogeneously and simultaneously. We measure the evolution of a quantum Ising ring and accurately reconstruct the Hamiltonian parameters, showcasing an accurate and high-fidelity simulation. Our method enables a significant reduction in the required control and depth of quantum simulations, thus generating longer evolution times with higher accuracy.

Quantum simulators are controllable quantum systems that enable the study of phases, dynamics, and properties of complex quantum systems, for which an analytical or numerical treatment is challenging [1]. Quantum simulations are considered a suitable task for noisy intermediate scale quantum (NISQ) computers [2], currently available. Indeed, recent years have seen numerous implementations of quantum simulations on several computing platforms [3–5], which are performed with an ever-increasing quality, approaching an advantage over classical methods [6]. An apparent challenge to NISQ-era computers is to perform large-scale quantum simulations, with a relatively shallow circuit depth, i.e. with few operations, in order to avoid the deterioration of the simulation's fidelity due to noise.

Ion-crystals trapped in radio frequency (RF) traps are an especially prolific tool for quantum simulations [7–16], due to their long coherence times [17], high-fidelity control [18–21] and rich connectivity [22–25]. By exploiting the long-range coupling between all ions in the ion-crystal, it is possible to perform simultaneous entanglement of many ions in the crystal, potentially increasing the efficacy of the simulation.

Here we experimentally implement quantum simulations of the Ising-spin model on a small-scale trapped ions quantum computer [26]. We evolve our system using global pulses, that drive the ions homogeneously, and nevertheless generate a desired inhomogeneous programmable interaction in each pulse, which is unconstrained by the one-dimensional (1D) linear geometry of the ion-chain. This is enabled by purposefully and simultaneously coupling to all modes of motion of the trapped ions crystal, in a controllable manner. We are able to simulate spin-Hamiltonians of the form,

$$H = \sum_{n,m=1}^N J_{n,m} \sigma_x^{(n)} \sigma_x^{(m)}, \quad (1)$$

with $\sigma_x^{(n)}$ a Pauli- x operator acting on the n th spin of a N

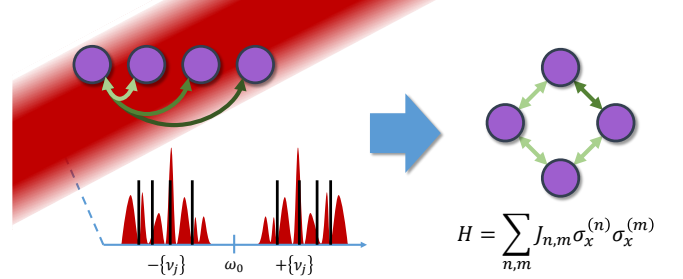


FIG. 1. Simulating spin-Ising Hamiltonians with trapped ions using a homogeneous drive. An ion chain (left) is driven by an approximately homogeneous drive, that has spectral contents overlapping the motional sidebands of the ion crystal, shown pictorially (bottom left). The motional modes generate tunable all-to-all couplings between all ions (e.g. the green arrows). By taking advantage of the motional mode structure the drive is mapped to a programmable Ising spin Hamiltonian (right). Here specifically we highlight a 4-spin ring that utilizes the inherent long-range coupling of the ions in order to generate anti-periodic boundary conditions, that are unconstrained by the linear geometry of the ion-crystal.

site spin system, and $J_{n,m}$ an experimentally controllable coupling matrix. This implements an Ising-spin model. Figure 1 pictorially presents our mapping from driving an ion-crystal to a simulation of an Ising-spin model.

With global methods that are straightforward in trapped ions systems, we extend this interaction to accommodate for a transverse field, $\delta \sum_{n=1}^N \sigma_z^{(n)}$. Similarly, we can add $\sigma_y^{(n)} \sigma_y^{(m)}$ terms, that may differ in their coupling matrix, compared to the coupling in Eq (1).

Our method takes into account and mitigates unwanted inhomogeneous aberrations due to, e.g. finite driving beam waist. Furthermore, while all modes of motion of the ion-crystal may be used, here we explicitly decouple from the center-of-mass mode as it is more prone to heating and decoherence, without affecting our method's programmability, thus improving the simula-

tion's fidelity.

We simulate a 4-ions Ising-spin quantum ring and observe dynamics under its Hamiltonian. We supplement this model with a transverse field, such that the resulting evolution is purely quantum mechanical, and observe the dynamics as a function of the transverse field magnitude.

Below we analyze these results in full, and are able to accurately reconstruct both the Ising coupling terms, $J_{n,m}$, as well as the various transverse fields, δ , showcasing an accurate realization of quantum simulations using our method.

The theoretical proposal underpinning our work has been proposed in Refs. [22, 23]. Here we provide the relevant physical picture and crucial details. In trapped-ions-based quantum computers, entanglement between qubits is typically generated by spin-dependent forces, which mediate spin-spin interactions through the collective phonon modes of motion of the ion-crystal. Conventionally only two ions are driven and coupled to a single phonon mode, such as in the Mølmer-Sørensen (MS) gate [27, 28], generating an evolution of the form $U_{\text{MS}} = \exp\left(i\Phi\sigma_x^{(n)}\sigma_x^{(m)}\right)$, with n and m the indices of the two entangled ions and Φ a controllable entanglement phase.

This method is generalized by homogeneously driving all of the N ions in the ion-crystal, purposefully coupling to N modes of motion along a motional axis of the ion-crystal. We have shown in Ref. [22] that such a drive can yield the evolution,

$$U = \exp\left(i\sum_{j=1}^N\Phi_j\sum_{n,m=1}^NO_j^{(n)}O_j^{(m)}\sigma_x^{(n)}\sigma_x^{(m)}\right), \quad (2)$$

with the $\{\Phi_j\}_{j=1}^N$ completely controllable mode-dependent entanglement phase, and O an orthonormal mode-matrix, i.e. $O_j^{(n)}$ is the normalized participation of the n th ion in the j th mode of motion [29].

We remark that the mapping between the Φ_j 's and the drive waveform that generates them involves solving a NP-hard optimization problem. In a different work we have presented a method for mitigating the hardness of this optimization problem [23]. Here however the optimization is circumvented by operating in a relevant adiabatic regime, detailed below.

Due to the orthonormality of O , shifting all Φ_j s by a constant, i.e. $\Phi_j \mapsto \Phi_j + \phi$, amounts to modifying U in Eq. (2) by a global phase, i.e. $U \mapsto e^{i\phi}U$. Here we exploit this property in order to set $\Phi_{j=1} = 0$, and adjust all the other Φ_j s appropriately. This is helpful as the $j = 1$ mode is a center-of-mass mode, which typically exhibits the fastest heating and decoherence rate. Thus, we are able to decouple from the center-of-mass mode completely, yielding longer coherence times and higher simulation fidelity.

Furthermore, we note that any inhomogeneity in the field driving the ions, e.g. due to a finite beam waist of an optical drive, can be taken into account by adjusting

O accordingly, thus enabling the mitigation of unwanted inhomogeneous effects.

In practice, in our setup the laser intensity is limited such that any single frequency can, at most, couple significantly to only a single mode of motion. In this low-power limit the gate operates in the adiabatic regime and the mapping between the desired entanglement phases and the corresponding drive is simple, relaxing the NP-hard problem described in Ref. [22].

Specifically, we drive two frequency pairs per motional mode, with the frequencies, $\omega_0 \pm (\nu_j + \xi)$ and $\omega_0 \pm (\nu_j + 3\xi)$, with ω_0 the single-qubit transition frequency, ν_j the frequency of the j th mode of motion and ξ a detuning determined below. The amplitude of both frequency pairs is equal and their phases are opposite. Following Ref. [30], these choices generate a robust gate that can be driven faster than the typical MS gate, as it reduces coupling to unwanted transitions such as off-resonance coupling to the carrier transition. Furthermore, the choice 3ξ (as opposed to, e.g. 2ξ) mitigates unwanted non-linear technical responses which may occur at the various hardware generating the laser's spectrum [31].

With these choices, we make use of consecutive implementations of U in Eq. (2), such that the ion's evolution, at integers multiples of $2\pi\xi^{-1}$, evolves stroboscopically according to the Hamiltonian in Eq. (1), with $J_{n,m} \propto \sum_{j=1}^N \frac{\eta_j^2 r_j^2}{\xi} O_j^{(n)} O_j^{(m)}$, such that η_j is the Lamb-Dicke parameter of the j th mode of motion, driven by the two-tone pairs described above, with a relative amplitude r_j . The proportionality constant accommodates for the laser's total Rabi frequency, Ω_0 , and additional (mode and ion independent) numerical factors [23].

The Pauli- x rotations, i.e. $\sigma_x^{(n)}$, in Eq. (2) can be trivially generalized to $\sigma_\phi^{(n)} = \cos(\phi)\sigma_x^{(n)} + \sin(\phi)\sigma_y^{(n)}$, with ϕ fully controllable, by equally shifting the average phase of all the frequency pairs constituting the drive by ϕ . The choice of ϕ , as well as all other drive parameters, i.e. the Φ_j s and ξ can be changed at each consecutive implementation of U . Combined with the well-known Suzuki-Trotter decomposition [32, 33], this accommodates for various spin-Hamiltonians, e.g.

$$H = \sum_{n,m=1}^N \left[J_{n,m}^{(x)} \sigma_x^{(n)} \sigma_x^{(m)} + J_{n,m}^{(y)} \sigma_y^{(n)} \sigma_y^{(m)} \right] + \delta \sum_{n=1}^N \sigma_z^{(n)}, \quad (3)$$

with $J_{n,m}^{(x)}$ and $J_{n,m}^{(y)}$ controllable couplings and δ a controllable transverse field. The $\sigma_y^{(n)}$ terms are generated by a $\pi/2$ jump in ϕ , while the transverse $\sigma_z^{(n)}$ terms are generated by a gradual linear ramp of ϕ in each consecutive Suzuki-Trotter block.

The general Hamiltonian in Eq. (3), as well as more elaborate, e.g. time-dependent Hamiltonians, are all made possible without breaking the global-drive assumption. We remark that H commutes with the parity operator $P = \exp\left(i\pi \sum_{n=1}^N \sigma_z^{(n)}\right)$, thus states with well-

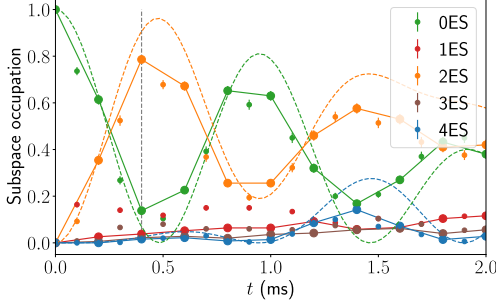


FIG. 2. Excitation subspace dynamics of the four site anti-periodic Ising-spin ring. Populations are measured at integer, up to ten, consecutive implementations of U (points connected by lines) as well as half-integer multiples (small points), and grouped into excitation subspaces. The theoretical prediction (dashed) shows a good agreement with the data. The system exhibits dynamics in even-excitation subspaces (green, orange, and blue), with a steady linear rise of population in odd-excitation subspaces (brown and red) due to experimental imperfections. Error bars reflect $\pm 2\sigma$ statistical errors due to quantum shot noise. Below we study further the system's state at an early evolution time (vertical dashed grey line).

defined parity, e.g. superpositions of states with an even number of spin-excitations, will remain with the same parity throughout their evolution.

We experimentally implement quantum simulations on a small-scale trapped-ions quantum computer [26], in which the $|5S_{\frac{1}{2}, \frac{1}{2}}\rangle$ ($|4D_{\frac{5}{2}, \frac{3}{2}}\rangle$) states of $^{88}\text{Sr}^+$ ions are mapped to $|0\rangle$ ($|1\rangle$) qubit levels. These levels are coupled, using a quadrupole transition, by a 674 nm narrow linewidth laser [34], illuminating the ions approximately homogeneously with a wide global beam. We modulate the 674 nm beam appropriately such that it has a rich spectrum, containing the frequency pairs, $\{\omega_0 \pm \omega_m\}_{m=1}^M$, with ω_0 the $|0\rangle \leftrightarrow |1\rangle$ transition frequency. This pairwise driving generates the spin-dependent forces, driving the modes of motion of the ion-crystal, and mediating the entangling interaction [22, 23].

We start by investigating dynamics under a 4-site spin ring, with anti-periodic boundary conditions, i.e. the nearest-neighbor ($n.n$) Hamiltonian,

$$H_{\text{ring,a.p}} = \Omega \left(\sigma_x^{(1)} \sigma_x^{(2)} + \sigma_x^{(2)} \sigma_x^{(3)} + \sigma_x^{(3)} \sigma_x^{(4)} - \sigma_x^{(4)} \sigma_x^{(1)} \right) + \delta \sum_{n=1}^4 \sigma_z^{(n)}, \quad (4)$$

with 'anti-periodicity' manifested as the negative sign of the $\sigma_x^{(4)} \sigma_x^{(1)}$ coupling term. As we show below, $H_{\text{ring,a.p}}$ can be well-approximated by the axial modes of motion of our harmonic ion-trap, with the choice $\{\Phi_j\}_{j=1}^4 \approx \{0, 0.3867, -0.7071, -1.0939\}$.

We first benchmark our simulation with $\delta = 0$. To do

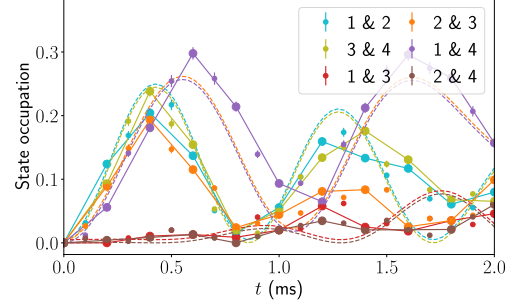


FIG. 3. Dynamics in post-selected 2 excitation subspace of a four-site anti-periodic Ising-spin ring (data and theory marked as in Fig. 2). A significant part of the evolution involves states that are nn in the model, i.e. the states $|1100\rangle$ (cyan), $|0110\rangle$ (orange), $|0011\rangle$ (olive) and $|1001\rangle$ (purple), with the latter manifested by ions which are at the two opposite edges of the ion-crystal. States that occupy nnn are significantly less populated throughout the evolution (red and brown). Error bars reflect $\pm 2\sigma$ statistical errors due to quantum shot noise.

so we initialize the system to the ground state, $|0000\rangle$, allow it to evolve under $H_{\text{ring,a.p}}$, and measure the population at the different spin states. Figure 2 shows the state occupations after such an evolution, with the spin populations grouped in terms of their respective excitation subspaces (ES), i.e. the number of excitations in each state. Data (points connected by lines) is accompanied by the theoretical expectation (dashed) showing a good agreement. We sample the evolution stroboscopically, at integer multiples of U (points connected by solid) as well as at half-integer multiples of U (small unconnected points). Error bars reflect $\pm 2\sigma$ statistical errors due to quantum shot noise. Here and in the measurements below we use $\xi = 7.5$ kHz.

Since the initial state (green) is in an even ES, we expect the system to only populate even ESs. Indeed we observe significant dynamics in the 2-ES (orange) and 4-ES (blue) subspaces. In addition, we note a small linear build-up of the population in the odd 1-ES (red) and 3-ES (brown), which is due to dephasing and experimental imperfections. Furthermore, we note that at half-integer multiples of U the populations in the odd ESs are significant even at small times, as these subspaces are essential in the dynamics in non-stroboscopic times [28].

A clear picture of the dynamics emerges by considering independently all the states in the 2-ES. Indeed Fig. 3 shows the evolution in these states. As we expect our models to conserve parity, we post-select our measured data by ignoring measurement results occupying odd ESs and renormalizing the recurrence of the remaining measured states. The dynamics show that the initial buildup of the population in the 2-ES is, in fact, dominated by states which are nn in the spin-ring, i.e. the states $|1100\rangle$ (cyan), $|0110\rangle$ (orange), $|0011\rangle$ (olive) and $|1001\rangle$ (purple), with the latter manifested by ions which are at the two opposite edges of the ion-crystal. Similarly,

states that occupy next-nearest-neighbor (*n.n.n*) sites, i.e. $|1010\rangle$ (red) and $|0101\rangle$ (brown), are only slightly populated at longer evolution times.

We quantify the simulation's performance by performing parity measurements. We do so by evolving the system for some small evolution time, $t_{\text{parity}} = 3\frac{2\pi}{\xi}$ (vertical dashed gray in Fig. 3), corresponding to three consecutive implementations of U , and then performing a global $\pi/2$ -pulse with phase ϕ . That is, the system evolves according to,

$$U_{\text{parity}} = e^{i\frac{\pi}{2} \sum_{n=1}^N \sigma_{\phi}^{(n)} U^3 |0000\rangle}, \quad (5)$$

after which we measure state occupations and evaluate the bipartite-parity, $\langle \sigma_z^{(n)} \sigma_z^{(m)} \rangle$. This process generates the measurement of the correlation, $C_{n,m}(\phi) = \langle \psi(t) | \sigma_{\phi}^{(n)} \sigma_{\phi}^{(m)} | \psi(t) \rangle$. The results of these measurements, for various rotation phases, ϕ , are shown in Fig. 4 (top). Similarly to the above, we note that sites that are *n.n* on the spin-ring (cyan, orange, olive, and purple) exhibit high-contrast parity fringes, while *n.n.n* sites (red, brown) do not. Furthermore $C_{1,4}$ (purple) exhibits an oscillation phase which is opposite to all others, due to its negative coupling.

To analyze the data further we use a single-parameter fit for each parity fringe shown in Fig. 4 as $C_{n,m}(\phi) \simeq J_{n,m}^{\text{reconstructed}} \sin(2\phi)$, showing a good fit (dashed). The resulting values of $J_{n,m}^{\text{reconstructed}}$ are presented in Fig. 4 (bottom, right), along with the ideal values of $J_{n,m}^{\text{ideal}}$ (bottom, left) which are directly read-off the model's Hamiltonian Eq. (4), as well as the expected values of the implemented model, $J_{n,m}^{\text{expected}}$ (bottom, center), originating from our estimation of the system's modes of motion [29] and our drive's parameters (middle). The three coupling matrices are in good agreement. There is a slight deviation between the ideal (left) and expected (middle) matrices in $J_{2,3} = J_{3,2}$ and $J_{1,4} = J_{4,1}$. We remark that $J_{n,m}^{\text{expected}}$ is used to generate the theoretical expectations of Figs. 2 and 3, scaled appropriately such that, $|J_{n,m}^{\text{expected}}| e^{-t_{\text{parity}}/T_2} = |J_{n,m}^{\text{reconstructed}}|$, with T_2 our system's coherence time.

We heuristically quantify our ability to realize this specific model by constructing an overlap between coupling matrices, $F(J_{n,m}, S_{n,m}) \equiv \mathbf{J} \cdot \mathbf{S} / \sqrt{(\mathbf{J} \cdot \mathbf{J})(\mathbf{S} \cdot \mathbf{S})}$, with \mathbf{J}, \mathbf{S} being 6-element real vectors constructed from the upper triangular entries of the coupling matrices (excluding the trivial diagonal). This overlap yields $F(J_{n,m}^{\text{ideal}}, J_{n,m}^{\text{expected}}) = 0.985$ and $F(J_{n,m}^{\text{expected}}, J_{n,m}^{\text{reconstructed}}) = 0.993$, indeed verifying a high-quality implementation of the intended ring model.

We now turn to study the effects of the transverse field, δ , in the ring Hamiltonian in Eq. (4). This term generates a global σ_z coupling which does not commute with the Ising *n.n* interaction.

At high transverse field value, i.e. $\delta/\Omega \gg 1$ the initial state, $|0000\rangle$ becomes an eigenstate. Thus, approaching this limit, we expect an effective slowing down of the

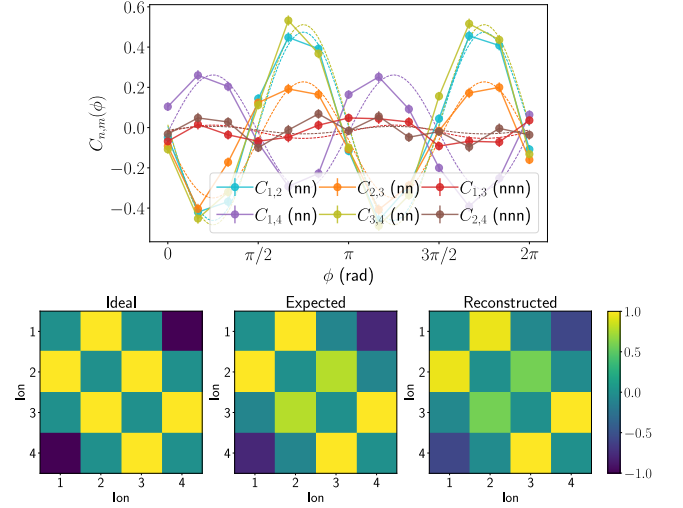


FIG. 4. Pair parity oscillations between sites of the four-site anti-periodic Ising-spin ring and coupling matrix reconstruction. Top: The correlation $C_{n,m} = \langle \sigma_{\phi}^{(n)} \sigma_{\phi}^{(m)} \rangle$ is evaluated between different pairs of the system, at various values of ϕ , after a small evolution time $t_{\text{parity}} = 6\pi\xi^{-1}$. We observe high-contrast oscillations between sites that are *nn*, and low-contrast oscillations between sites that are *nnn*. The anti-periodic negative coupling of $\sigma_x^{(1)} \sigma_x^{(4)}$ in Eq. (4), is manifested as an opposite phase fringe of $C_{1,4}$ (purple) compared to all others. Error bars reflect $\pm 2\sigma$ statistical errors due to quantum shot noise. Data (points connected by lines) is fitted to a single oscillating sine (dashed) showing a good fit. Bottom: coupling matrices, $J_{n,m}$, of the four-site anti-periodic Ising-spin ring. Showing its ideal values (left) read-off the model's Hamiltonian in Eq. (4), the expected values (middle) due to a global drive implementation, and the reconstructed values (right), using the parity fits (top). The matrices are normalized such that the largest entry in each of them is 1 (arbitrary units).

observed dynamics. We quantify an effective coupling, $\tilde{\Omega}$, from our measurements above as the average observed *nn* coupling (in absolute value), i.e.

$$\tilde{\Omega}t = \frac{1}{4} \sum_{n=1}^4 |J_{n,n+1}^{\text{reconstructed}}|, \quad (6)$$

with $4+1 \mapsto 1$. Figure 5, shows the post-selected populations in even excitation subspaces (points connected by lines), for various choices of $\delta/\tilde{\Omega}$ (color bars). Indeed, the ground state population (green lines) remains more populated throughout the observed dynamics for larger values (brighter) of $\delta/\tilde{\Omega}$, while two excitations (orange) and four excitations (blue) become less frequent.

To analyze the data further, and benchmark our simulation, we consider the population in the ground state, $\text{Pr}(0000)$, after two consecutive applications of U in Eq. (2) and a single application of the transverse field term (dashed gray line). We heuristically model the expected system excitations using the well-known formula for off-

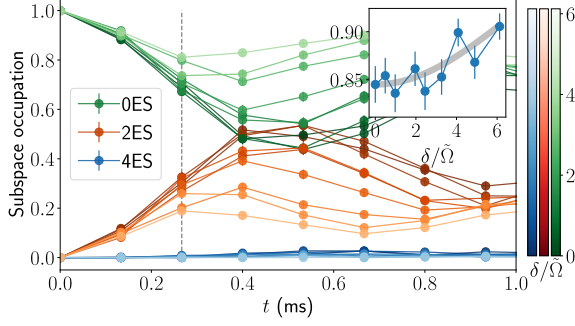


FIG. 5. Dynamics of a four-site anti-periodic Ising-spin ring, with an on-site homogeneous transverse field. We prepare the state $|0000\rangle$ and evolve it under the system's Hamiltonian. Populations of the various system states are measured at different evolution times (points) and grouped according to the number of excitations, with no excitation (green), two excitations (red) and four excitations (blue). We repeat this measurement for various ratios of transverse field to Ising-type nearest neighbor coupling, $\delta/\tilde{\Omega}$ (color bars). For large transverse fields the initial state becomes an eigenstate, leading to a suppression of dynamics. Error bars reflect 2σ errors due to quantum shot noise. Inset: Measured ground state population (blue) after a short evolution time, $t = 4\pi\xi^{-1}$ (dashed vertical grey), compared to the prediction of Eq. (7) (grey), showing a good fit.

resonance Rabi oscillations, $\frac{1}{1+\frac{\delta^2}{\Omega_0^2}} \sin^2\left(\frac{1}{2}\Omega_0 t \sqrt{1+\frac{\delta^2}{\Omega_0^2}}\right)$, at time t coupled by a Rabi frequency Ω_0 which is detuned by δ . Here we replace $\Omega_0 \mapsto 4\tilde{\Omega}$ as there are four relevant states in the two excitations subspace. Furthermore, as we have used 2 applications of the Ising interaction and a single application of the transverse field, we choose $t = \frac{3}{2}\Omega_0^{-1}$. Thus we estimate,

$$1 - \text{Pr}(0000) = \frac{1}{1 + \frac{\delta^2}{(4\tilde{\Omega})^2}} \sin^2\left(3\tilde{\Omega} \sqrt{1 + \frac{\delta^2}{(4\tilde{\Omega})^2}}\right). \quad (7)$$

Figure 5 (inset) shows the measured ground state pop-

ulation (blue), extracted after the second application of U . We also plot our estimate in Eq. (7) (grey) showing a good fit. We remark that in order to account for experimental imperfections, e.g. the system's coherence, we have scaled the expression of our estimate in Eq. (7) such that it exactly matches our first data point at $\delta = 0$, with no other fitting parameters. Thus we are able to deduce the transverse field used in our realizations, over a large range of values.

In conclusion, we have demonstrated a method for programmable quantum simulations of spin-Hamiltonians on trapped-ion chains. The method, proposed in Ref. [22], can be used to generate a variety of models and coupling geometries, which are unconstrained by the physical realization of the 1D linear ion-crystal. Here we employ it to generate a 4-site anti-periodic Ising-spin ring. We use population and correlation data in order to benchmark our simulation. Indeed we reconstruct the applied couplings and transverse field, showing a faithful generation of the intended model. This method is well-suited for NISQ-era quantum systems as it can be used to leverage typical shallow circuits yet still generate long evolution times of relevant quantum systems.

During the preparation of this manuscript we became aware of a similar work by Wu et al. [16], which uses similar techniques in order to implement similar Ising models.

ACKNOWLEDGMENTS

This work was supported by the Israeli Science Foundation, the Israeli Ministry of Science Technology and Space, the Minerva Stiftung, the European Union's Horizon 2020 research and innovation programme (Grant Agreement LEGOTOP No. 788715), the DFG (CRC/Transregio 183, EI 519/7-1), ISF Quantum Science and Technology (2074/19).

-
- [1] R. P. Feynman, Simulating physics with computers, *International Journal of Theoretical Physics* **21**, 467 (1982).
 - [2] J. Preskill, Quantum Computing in the NISQ era and beyond, *Quantum* **2**, 79 (2018).
 - [3] C. Neill, T. McCourt, X. Mi, Z. Jiang, M. Y. Niu, W. Mruczkiewicz, I. Aleiner, F. Arute, K. Arya, J. Atalaya, R. Babbush, J. C. Bardin, R. Barends, A. Bengtsson, A. Bourassa, M. Broughton, B. B. Buckley, D. A. Buell, B. Burkett, N. Bushnell, J. Campero, Z. Chen, B. Chiaro, R. Collins, W. Courtney, S. Demura, A. R. Derk, A. Dunsworth, D. Eppens, C. Erickson, E. Farhi, A. G. Fowler, B. Foxen, C. Gidney, M. Giustina, J. A.

- Gross, M. P. Harrigan, S. D. Harrington, J. Hilton, A. Ho, S. Hong, T. Huang, W. J. Huggins, S. V. Isakov, M. Jacob-Mitos, E. Jeffrey, C. Jones, D. Kafri, K. Kechedzhi, J. Kelly, S. Kim, P. V. Klimov, A. N. Korotkov, F. Kostritsa, D. Landhuis, P. Laptev, E. Lucero, O. Martin, J. R. McClean, M. McEwen, A. Megrant, K. C. Miao, M. Mohseni, J. Mutus, O. Naaman, M. Neeley, M. Newman, T. E. O'Brien, A. Opremcak, E. Ostby, B. Pató, A. Petukhov, C. Quintana, N. Redd, N. C. Rubin, D. Sank, K. J. Satzinger, V. Shvarts, D. Strain, M. Szalay, M. D. Trevithick, B. Villalonga, T. C. White, Z. Yao, P. Yeh, A. Zalcman, H. Neven, S. Boixo, L. B. Ioffe, P. Roushan, Y. Chen, and V. Smelyanskiy, Accu-

- rately computing the electronic properties of a quantum ring, *Nature* **594**, 508 (2021).
- [4] Y. Kim, A. Eddins, S. Anand, K. X. Wei, E. van den Berg, S. Rosenblatt, H. Nayfeh, Y. Wu, M. Zaletel, K. Temme, and A. Kandala, Evidence for the utility of quantum computing before fault tolerance, *Nature* **618**, 500 (2023).
 - [5] G. Semeghini, H. Levine, A. Keesling, S. Ebadi, T. T. Wang, D. Bluvstein, R. Verresen, H. Pichler, M. Kalinowski, R. Samajdar, A. Omran, S. Sachdev, A. Vishwanath, M. Greiner, V. Vuletić, and M. D. Lukin, Probing topological spin liquids on a programmable quantum simulator, *Science* **374**, 1242 (2021), <https://www.science.org/doi/pdf/10.1126/science.abi8794>.
 - [6] K. Kechedzhi, S. V. Isakov, S. Mandrà, B. Villalonga, X. Mi, S. Boixo, and V. Smelyanskiy, Effective quantum volume, fidelity and computational cost of noisy quantum processing experiments (2023), [arXiv:2306.15970 \[quant-ph\]](https://arxiv.org/abs/2306.15970).
 - [7] T. Manovitz, Y. Shapira, N. Akerman, A. Stern, and R. Ozeri, Quantum simulations with complex geometries and synthetic gauge fields in a trapped ion chain, *PRX Quantum* **1**, 020303 (2020).
 - [8] Y. Shapira, T. Manovitz, N. Akerman, A. Stern, and R. Ozeri, Quantum simulations of interacting systems with broken time-reversal symmetry, *Phys. Rev. X* **13**, 021021 (2023).
 - [9] C. Kokail, C. Maier, R. van Bijnen, T. Brydges, M. K. Joshi, P. Jurcevic, C. A. Muschik, P. Silvi, R. Blatt, C. F. Roos, *et al.*, Self-verifying variational quantum simulation of lattice models, *Nature* **569**, 355 (2019).
 - [10] M. K. Joshi, F. Kranzl, A. Schuckert, I. Lovas, C. Maier, R. Blatt, M. Knap, and C. F. Roos, Observing emergent hydrodynamics in a long-range quantum magnet, *Science* **376**, 720 (2022).
 - [11] W. L. Tan, P. Becker, F. Liu, G. Pagano, K. S. Collins, A. De, L. Feng, H. B. Kaplan, A. Kyprianidis, R. Lundgren, W. Morong, S. Whitsitt, A. V. Gorshkov, and C. Monroe, Domain-wall confinement and dynamics in a quantum simulator, *Nature Physics* **17**, 742 (2021).
 - [12] A. Kyprianidis, F. Machado, W. Morong, P. Becker, K. S. Collins, D. V. Else, L. Feng, P. W. Hess, C. Nayak, G. Pagano, *et al.*, Observation of a prethermal discrete time crystal, *Science* **372**, 1192 (2021).
 - [13] M. Qiao, Z. Cai, Y. Wang, B. Du, N. Jin, W. Chen, P. Wang, C. Luan, E. Gao, X. Sun, H. Tian, J. Zhang, and K. Kim, Observing frustrated quantum magnetism in two-dimensional ion crystals, *arXiv preprint arXiv:2204.07283* [10.48550/ARXIV.2204.07283](https://arxiv.org/abs/2204.07283) (2022).
 - [14] M. Iqbal, N. Tantivasadakarn, R. Verresen, S. L. Campbell, J. M. Dreiling, C. Figgatt, J. P. Gaebler, J. Johansen, M. Mills, S. A. Moses, J. M. Pino, A. Ransford, M. Rowe, P. Siegfried, R. P. Stutz, M. Foss-Feig, A. Vishwanath, and H. Dreyer, Creation of non-abelian topological order and anyons on a trapped-ion processor (2023), [arXiv:2305.03766 \[quant-ph\]](https://arxiv.org/abs/2305.03766).
 - [15] D. Porras and J. I. Cirac, Effective quantum spin systems with trapped ions, *Phys. Rev. Lett.* **92**, 207901 (2004).
 - [16] Q. Wu, Y. Shi, and J. Zhang, Qubits on programmable geometries with a trapped-ion quantum processor (2023), [arXiv:2308.10179 \[quant-ph\]](https://arxiv.org/abs/2308.10179).
 - [17] P. Wang, C.-Y. Luan, M. Qiao, M. Um, J. Zhang, Y. Wang, X. Yuan, M. Gu, J. Zhang, and K. Kim, Single ion qubit with estimated coherence time exceeding one hour, *Nature Communications* **12**, 233 (2021).
 - [18] J. P. Gaebler, T. R. Tan, Y. Lin, Y. Wan, R. Bowler, A. C. Keith, S. Glancy, K. Coakley, E. Knill, D. Leibfried, and D. J. Wineland, High-fidelity universal gate set for $^9\text{Be}^+$ ion qubits, *Phys. Rev. Lett.* **117**, 060505 (2016).
 - [19] C. R. Clark, H. N. Tinkey, B. C. Sawyer, A. M. Meier, K. A. Burkhardt, C. M. Seck, C. M. Shappert, N. D. Guise, C. E. Volin, S. D. Fallek, H. T. Hayden, W. G. Rellergert, and K. R. Brown, High-fidelity bell-state preparation with $^{40}\text{Ca}^+$ optical qubits, *Phys. Rev. Lett.* **127**, 130505 (2021).
 - [20] C. J. Ballance, T. P. Harty, N. M. Linke, M. A. Sepiol, and D. M. Lucas, High-fidelity quantum logic gates using trapped-ion hyperfine qubits, *Phys. Rev. Lett.* **117**, 060504 (2016).
 - [21] R. Srinivas, S. C. Burd, H. M. Knaack, R. T. Sutherland, A. Kwiatkowski, S. Glancy, E. Knill, D. J. Wineland, D. Leibfried, A. C. Wilson, D. T. C. Allcock, and D. H. Slichter, High-fidelity laser-free universal control of trapped ion qubits, *Nature* **597**, 209 (2021).
 - [22] Y. Shapira, R. Shaniv, T. Manovitz, N. Akerman, L. Peleg, L. Gazit, R. Ozeri, and A. Stern, Theory of robust multiqubit nonadiabatic gates for trapped ions, *Phys. Rev. A* **101**, 032330 (2020).
 - [23] Y. Shapira, L. Peleg, D. Schwerdt, J. Nemirovsky, N. Akerman, A. Stern, A. B. Kish, and R. Ozeri, Fast design and scaling of multi-qubit gates in large-scale trapped-ion quantum computers (2023), [arXiv:2307.09566 \[quant-ph\]](https://arxiv.org/abs/2307.09566).
 - [24] N. Grzesiak, R. Blümel, K. Wright, K. M. Beck, N. C. Pienti, M. Li, V. Chaplin, J. M. Amini, S. Debnath, J.-S. Chen, and Y. Nam, Efficient arbitrary simultaneously entangling gates on a trapped-ion quantum computer, *Nature Communications* **11**, 2963 (2020).
 - [25] K. Wang, J.-F. Yu, P. Wang, C. Luan, J.-N. Zhang, and K. Kim, Fast multi-qubit global-entangling gates without individual addressing of trapped ions, *Quantum Science and Technology* **7**, 044005 (2022).
 - [26] T. Manovitz, Y. Shapira, L. Gazit, N. Akerman, and R. Ozeri, Trapped-ion quantum computer with robust entangling gates and quantum coherent feedback, *PRX Quantum* **3**, 010347 (2022).
 - [27] A. Sørensen and K. Mølmer, Quantum computation with ions in thermal motion, *Phys. Rev. Lett.* **82**, 1971 (1999).
 - [28] A. Sørensen and K. Mølmer, Entanglement and quantum computation with ions in thermal motion, *Phys. Rev. A* **62**, 022311 (2000).
 - [29] D. F. V. James, Quantum dynamics of cold trapped ions with application to quantum computation, *Applied Physics B* **66**, 181 (1998).
 - [30] Y. Shapira, R. Shaniv, T. Manovitz, N. Akerman, and R. Ozeri, Robust entanglement gates for trapped-ion qubits, *Phys. Rev. Lett.* **121**, 180502 (2018).
 - [31] J. Markov, Y. Shapira, N. Akerman, and R. Ozeri, Digital predistortion of optical field of a fast and high-fidelity entangling gate for trapped ions qubits (2023), 54th Annual Meeting of the APS Division of Atomic, Molecular and Optical Physics.
 - [32] H. F. Trotter, On the product of semi-groups of operators, *Proceedings of the American Mathematical Society* **10**, 545 (1959).
 - [33] M. Suzuki, Generalized trotter's formula and systematic approximants of exponential operators and inner deriva-

- tions with applications to many-body problems, *Communications in Mathematical Physics* **51**, 183 (1976).
- [34] L. Peleg, N. Akerman, T. Manovitz, M. Alon, and R. Ozeri, Phase stability transfer across the optical domain using a commercial optical frequency comb system (2019), [arXiv:1905.05065 \[physics.atom-ph\]](#).